Understanding the activity of Zn-Cu sites in methanol synthesis

Batyrev, E.D.

Publication date
2013

Chapter 5

Modification of the ZnO (0001)-Zn surface under reducing conditions*

Abstract

The ZnO (0001)-Zn terminated crystal face was studied after reduction at high temperatures by combination of Scanning Tunneling Microscopy, Scanning Tunneling Spectroscopy, X-ray Photoelectron Spectroscopy (XPS) and Thermal Desorption Spectroscopy. The clean ZnO (0001)-Zn surface exhibits triangular reconstruction in UHV, while after exposure to 10^{-5} mbar H_2 at RT this reconstruction is lifted and a rough surface has formed. The roughness as well as the metallic character of the surface increased with the applied low-pressure reduction temperature up to 800 K. XPS revealed that exposure to 1 bar H_2 at RT led to the formation of OH groups; at higher temperatures progressive metallization of the ZnO surface was found to occur. Analysis of the thermal desorption results showed that huge amounts of H_2 dissolved into the ZnO crystal. The results obtained under these conditions were in good accordance with thermodynamic calculations. The experimental ratio between the absorbed amount of H_2 at RT and 800 K amounts to 1000. The ratio calculated from increasing diffusion coefficients with temperature only amounts to 6. This emphasizes the importance of ZnO as a H supplier by spillover, and proves that metallic Zn boosts dissociative adsorption of H_2. This surface modification of ZnO structure during the reduction promotes an enhanced activity of the Cu/ZnO catalyst at elevated temperatures.

5.1 Introduction

Cu-ZnO based catalysts are very active and selective in methanol synthesis, but the reaction mechanism and nature of active sites are still under debate [1-7]. It is known that ZnO plays an important role which ranges from hydrogen supplier by spillover [1-3] to anti-sintering agent [4, 5], and even a role as an active site [6, 7].

*E.D. Batyrev and J.C. van de Heuvel, *Phys. Chem. Chem. Phys.*, 2011, 13, 13127.

As reported already [8] the reduction at 750 K strongly enhanced the activity of the ZnO promoted Cu catalyst. Little information is available about the surface structure of the catalyst, particularly the ZnO phase, after reduction in hydrogen at high temperature. This study is devoted to the characterisation of the activated catalyst surface that catalyses the hydrogenation of CO/CO_2.

In polycrystalline catalysts Bowker and co-workers found that the polar faces are rather active in the methanol synthesis as compared to non-polar faces [9].

Later, Vohs and Barteau proved that the ZnO $(000\bar{1})$-O terminated face is completely inactive in this reaction [10]. Therefore, the polar ZnO (0001)-Zn terminated surface was chosen for this single crystal study as the most active face in polycrystalline powder catalysts.

In the case of polar surfaces where a dipole moment is perpendicular to the surface a further reconstruction of the surface is required [11]. Kresse *et al.* concluded that depending on the hydrogen pressure, ZnO (0001)-Zn exhibits either triangular shaped reconstructions or remains a flat, unreconstructed face covered by hydroxyl groups [12]. Later, Valtiner *et al.* reported about hydroxide stabilised ZnO (0001)-Zn-OH surfaces prepared under ambient conditions [13]. From a catalytic point of view the regime where OH groups and triangular reconstructions compete in stability might be interesting. Thus, detailed information is needed to understand the processes on this ZnO surface before the metal-deposited Cu/ZnO model catalysts for methanol synthesis can be studied. In this investigation on the ZnO (0001)-Zn surface under reducing conditions a combination of surface science techniques such as scanning tunneling microscopy (STM), scanning tunneling spectroscopy (STS), X-ray photoelectron spectroscopy (XPS) and thermal desorption spectroscopy (TDS) was applied.

5.2 Zinc oxide

ZnO is a widely used *n*-semiconductor with a wide band-gap of 3.2 eV at 300 K. To a large extent its electrical and chemical properties depend on various defects such as Zn interstitials (Zn_i) and O vacancies (V_O). ZnO has a tetrahedral coordination formed by sp^3 hybridised orbitals and exhibits a hexagonal wurtzite structure, in which the direction of each apex is parallel to the [14] polar *c*-axis. That is the reason why ZnO tends to grow towards the [0001] direction, and the perpendicularly oriented (0001) plane is easy to create. Fujimura *et al.* calculated that among the low index planes the (0001) plane has the lowest surface free energy of 99 meV/Å^2 [15].

This means that the (0001) plane will be the most favourable plane in polycrystalline ZnO powder.

At a base pressure of 10^{-10} mbar, a clean ZnO (0001)-Zn surface consists of triangular islands and pits with monolayer step height [16] or facets in the form of highly regular step arrays when being annealed above 1150 K [17]. The opposite side of the crystal is an O-terminated face. Within the ionic model it is clear that a dipole moment is generated perpendicular to perfectly flat polar faces, while the internal field in the single crystal cancels for reasons of symmetry [18]. Electrostatic arguments indicate that such surfaces cannot exist and their apparent natural occurrence has been associated with substantial reconstruction or adsorption of additional charge [19, 20]. Such a reconstruction requires a compensating charge transfer of ½ e^- from the O- to the Zn-terminated face, leading to formal surface charges of $Zn^{1.5+}$ and $O^{1.5-}$.

Dulub *et al.* reported that the removal of 25 % Zn from the surface is required for stabilization, thereby exposing the oxygen atoms at the step edges of the triangular islands and pits [21]. This is consistent with surface XRD measurements on ZnO (0001)-Zn by Jedrecy *et al.* [22], which could be best fitted by removing randomly 25% of the Zn atoms, i.e. formation of ¼ ML zinc vacancies (V_{Zn2+}). As a consequence, all step edges are decorated by oxygen atoms.

Recently, Torbrügge *et al.* [23] proposed a novel stabilization phase of ZnO (0001)-Zn surface by a (1 × 3) surface reconstruction consisting of missing Zn-rows. That brings new insights on ZnO interaction with hydrogen.

There is an energetic competition between the formation of isolated Zn vacancies and triangular reconstruction. The calculations of Kresse *et al.* [12] indicate that larger triangles with smaller inner triangles (rotated 180°) are favoured, and that the energetically most favourable triangle is 6 sites wide. The stability of the triangular reconstruction is governed by the Madelung energy. O atoms have a repulsive 2nd coordination shell of 6 in the unreconstructed surface, which is reduced to 4-5 for the triangles.

The excess electrons in the conduction band can also be removed by the formation of ½ ML OH^- upon exposure to hydrogen. The above cited work of Kresse *et al.* [12] reveals that the specific dissociative adsorption energy of H atop Zn atoms:

$$E_{ads} = (E_{slab|nH} - E_{slab} - \tfrac{1}{2}n\, E_{H2})/n < 0$$

is favourable up to a coverage of $\Theta = ½$ ML. This hydrogen adsorbed at the Zn atoms is thermodynamically unstable, since the reaction:

$$n\ ZnO + slab|nH \Rightarrow slab|nOH + n\ hcp\ Zn \qquad (1)$$

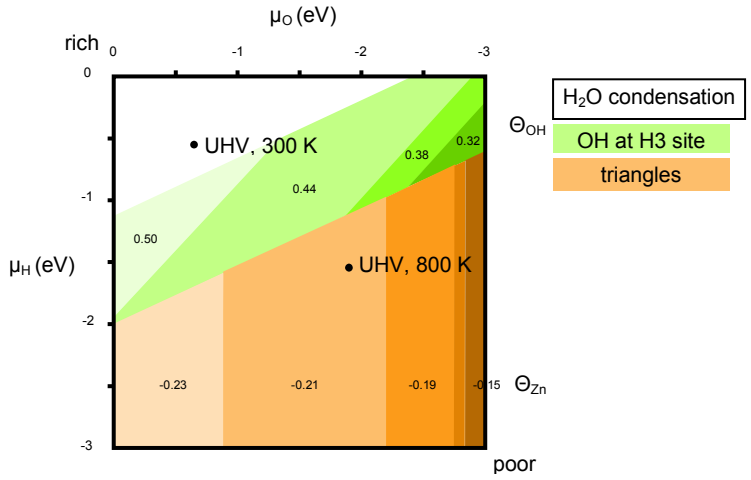

Fig. 1. *Phase diagram of the ZnO (0001)-Zn surface as a function of the chemical potentials μ_H and μ_O. Positive numbers indicate the OH coverage Θ_{OH}, negative numbers the Zn deficiency Θ_{Zn} per unit area; after Kresse et al. [12]. UHV refers to a pressure of 10^{-10} mbar. The experimental regimes of this work are indicated with the black dots.*

is exothermic. Thus hydrogen will reduce ZnO to metallic Zn, forming stable OH groups adsorbed at the threefold coordinated surface sites under the conditions indicated in the phase diagram (Fig. 1) [12]. Experimentally it was confirmed that H adsorption is exothermic on the Zn-terminated side and destroys the lateral order of the ZnO crystal because of the required O transport from the subsurface. Depletion of the Zn 4s state by OH coverage should be identifiable by XPS. At an OH^- coverage $\Theta > ½$ ML, the ionic OH^- contribution changes into the less favourable covalent OH bonding.

After dissociative adsorption, H will also penetrate into the ZnO subsurface [2, 3, 24-26]. When a H atom enters the ZnO lattice its ionization energy decreases from 13.59 eV to a shallow donor level of 0.05 eV because of the strong electric field in ZnO [27-29]. Therefore, the proton-electron bond length will increase accordingly from 0.7 to 30 Å [30]. Due to band bending at the positively charged Zn-terminated surface electrons will be injected into the conduction band even at temperatures as low as 100 K [14, 31, 32], changing the electronic configuration of the semiconductor towards a metal. DFT calculations by Van de Walle indicate that the protons will preferentially locate at interstitial positions between fully-coordinated O and Zn atoms. This weakens their bond, and the associated lattice

displacement of the Zn atoms for the bond-center configuration was computed as 40 % (0.8 Å) of the bond length [29].

Quantitative LEED measurements on the ZnO polar surfaces have indicated that the outer Zn-terminated layer is relaxed inward by 0.2 Å, while the O-terminated face did not show any contraction [11]. Such a difference was to be expected considering the larger size of the O^{2-} ion (1.4 Å) as compared to the Zn^{2+} ion (0.74 Å). Based on surface X-ray diffraction data, Wander *et al.* demonstrated that the ZnO $(000\bar{1})$-O surface is unreconstructed [33]. This finding is supported by STM images, which show no defects other than steps [34].

The present study is devoted to the influence of reducing conditions on the structure of ZnO, being the support in our model system.

5.3 Experimental

The work was performed with a Multiprobe XP ultra high vacuum (UHV) Omicron system (Fig. 2) [35]. It consists of four chambers: load-lock, preparation chamber, analysis chamber, and a home-made reaction chamber. The sample is inserted to the UHV system *via* a fast entry load-lock and transported between the chambers by magnetic manipulators and wobble sticks.

The preparation chamber accommodates an ISE-10 ion source, EFM-3 evaporators and a heating stage (Fig. 2). Furthermore, a Prisma-80 QMS-200 Balzers quadrupole mass spectrometer (MS) is attached to the preparation chamber to monitor the gas composition, and to perform thermal desorption spectroscopy (TDS).

The main analysis chamber (Fig. 2) is equipped with a DAR-400 X-ray source and an EA-125 hemispherical analyzer to perform X-ray photoelectron spectroscopy (XPS). A bolt-on analysis chamber contains a variable temperature combined scanning tunneling (STM), as well as a six compartment carousel for samples and tips. The preparation and analysis chambers are equipped with a titanium sublimation pump (TSP) and an ion-getter pump (IGP); the X-ray source has an additional IGP pump. The base pressure during the experiments was in a range of $2\text{-}3\cdot10^{-10}$ mbar.

The chambers can be separated with valves in case of large pressure differences. This especially happens during treatments of the sample in the preparation chamber. For instance, to perform Ar^+ sputtering a leak valve between an Ar filled tube and the preparation chamber should be slightly open until the pressure in preparation chamber is stabilized at $3.5\cdot10^{-6}$ mbar while the valve between the analysis chamber and the preparation chamber is closed.

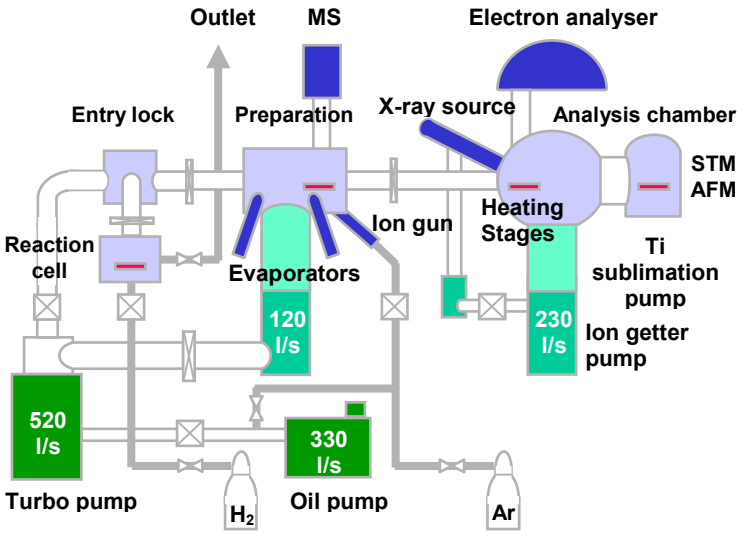

Fig. 2. *Scheme of the Multiprobe XP Omicron system [35].*

The home-made reaction chamber (Fig. 2) includes a leak valve, ion gauge pressure meter and a heating stage, and allows the exposure of sample to gases at relatively high pressures and temperatures. The pressure in the reaction cell should not exceed 1.2 bar because of the view port window, while the temperature is limited to 900 K due to the heating power. Thus, conditions comparable to those in the thermobalance setup [8] can be imposed, which allows to perform similar reduction treatments. The H_2 and Ar gases used were of 5.0 high purity. Connecting gas tubes were baked out at 473 K while pumping for 30 minutes and then flushed 3 times with H_2 or Ar at RT. Finally, after such cleaning procedure the lines were filled with the gas.

The mechanically cut and polished ZnO (0001) single crystals from hydrothermal origin were obtained from Surface Preparation Lab in Zaandam, The Netherlands. The $1.0 \times 1.0 \times 0.1$ cm^3 samples were fixed on an Omicron sample plate by a special frame with four screws; all parts are made of molybdenum or tantalum that allows the use of elevated temperatures. To characterize the roughness of a surface quantitatively, the root mean square (rms) roughness was taken throughout. The roughness of the polished surface amounted to 49 Å over an 800×800 nm^2 area. The STM image was processed using the slope method in order to subtract the background. This slope subtraction routine calculates the mean slopes of each line and/or column and subtracts these from the respective

line/column of the original data set. This calculation was done on the whole frame. The method works generally very well with most surface types and is less drastic than the mean subtraction method. Scala Pro 4.1 Omicron software was used to obtain and process STM images [35].

STM tips were made either by electrochemical etching of tungsten wire in aqueous NaCl solution or by cutting a Pt/Ir wire [35]. The freshly prepared tips were fixed tightly in the tube of an Omicron tip holder that was subsequently mounted on a special transport device. Sometimes an old STM tip was resharpened by Ar^+ sputtering.

All STM images were taken with a bias voltage V_b = +3.0 V and a tunneling current I_t = 1.0 nA, although before scanning the bias was set at +6.0 V to obtain a stable tip approach.

Scanning tunneling spectroscopy (STS) was used to probe the local electronic structure of the sample surface. To this end, scanning is stopped after moving the tip to a desired feature. Subsequently, the feedback loop is switched off and a voltage ramp is applied while measuring the concomitant current to produce a local I-V curve.

The polarity of the crystal faces was established by the etching rate of a 10% HCl solution as suggested by Mariano [36]. Samples were cleaned with acetone in an ultrasonic bath before insertion into the UHV setup. Subsequently, they were prepared for surface analysis in the preparation chamber. A typical cleaning cycle consists of Ar^+ sputtering for 20 minutes ($3.5 \cdot 10^{-6}$ mbar, 1 keV, 10 mA) followed by annealing at 1000 K in UHV for 15 minutes. The single crystals were heated radiatively, and the temperature was monitored by a thermocouple spot-welded on the heating stage. The temperature difference between heating stage and the sample holder was taken into account [35], and subtracted from the readings of the thermocouple. For the last cycle preceding the STM measurement, the sputtering time and annealing time were taken 10 and 5 minutes, respectively. A typical preparation procedure takes 15-20 cycles until the contamination level is lower than the XPS detection limit, while the roughness is about 5 Å over a 200 × 200 nm^2 area.

XPS spectra were obtained using Al K_α radiation (1486.6 eV), and were collected by Spectra software and subsequently processed by the XPSPEAK and CasaXPS program.

Samples were exposed to 1 bar H_2 in the reaction cell for 1 h at different temperatures up to 800 K. After cooling down in the H_2 atmosphere, the hydrogenated ZnO samples were transferred to the preparation chamber and heated in UHV from RT to 1000 K at 0.3 K/s. The composition of the desorbing species was monitored with the MS. Contributions from a similarly treated bare sample plate and

the heating stage, although small, were subtracted from the TDS curves of the reduced ZnO. About 10 minutes prior to the thermal desorption measurements, the TSP and IGP pumps were switched off to exclude any desorption from hot filaments. The preparation chamber was pumped by the turbo-molecular pump with a speed of 520 l/s to minimize re-adsorption.

5.4 Results and discussion

5.4.1 Scanning Tunnelling: Microscopy and Spectroscopy

As can be seen from the STM images presented in Fig. 3, the clean ZnO (0001)-Zn surface exhibits terraces with the typical triangular reconstruction. The observed terraces have multiple islands and pits with a monoatomic step height of 2.6 Å, which is precisely the same value as known from structural studies on ZnO [37].

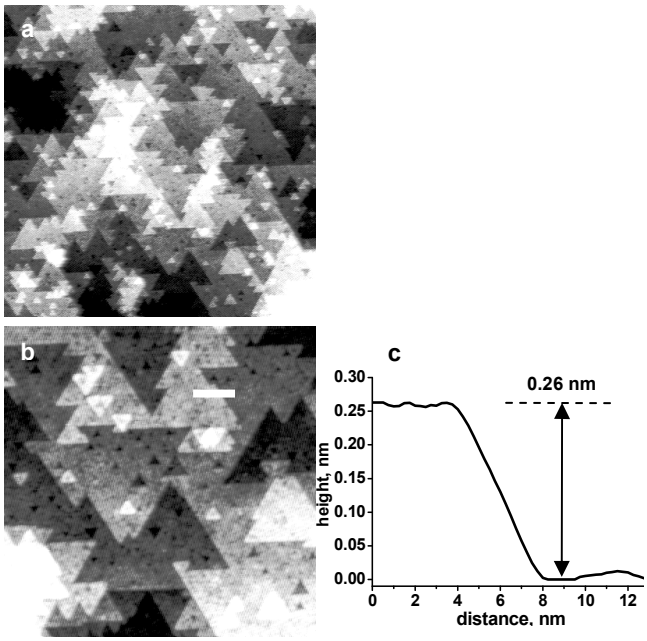

Fig. 3. *STM images of clean ZnO (0001)-Zn: a) 250 x 250 nm^2; b) 100 x 100 nm^2; c) line profile indicating the step height in Fig. 3b.*

After the preparation step the clean ZnO surface was exposed to 10^{-5} mbar H_2 at different temperatures, referred to as low-pressure reduction temperatures. It should be noticed that for each reduction treatment a clean ZnO surface was freshly prepared.

Exposure of the clean ZnO surface to 10^{-5} mbar H_2 for 30 minutes causes tremendous changes of the triangular surface structure into rough and irregular patterns (Fig. 4). From this result it can immediately be concluded that the triangular reconstruction of the ZnO (0001)-Zn surface cannot play any role in catalytic CO/CO_2 reduction. The increased surface roughness, though, might be relevant because of the associated structural defects such as islands and kinks. This roughness was found to increase with the low-pressure reduction temperature and has a maximum at 800 K (Fig. 5). Otherwise, different low-index planes will be exposed that are similar to those in a polycrystalline ZnO powder. The roughness of the sample exposed to 10^{-5} mbar H_2 at 900 K has decreased, probably because at such a high temperature the atoms are mobile enough to minimise the surface free energy. This temperature is 100 K higher than the optimal

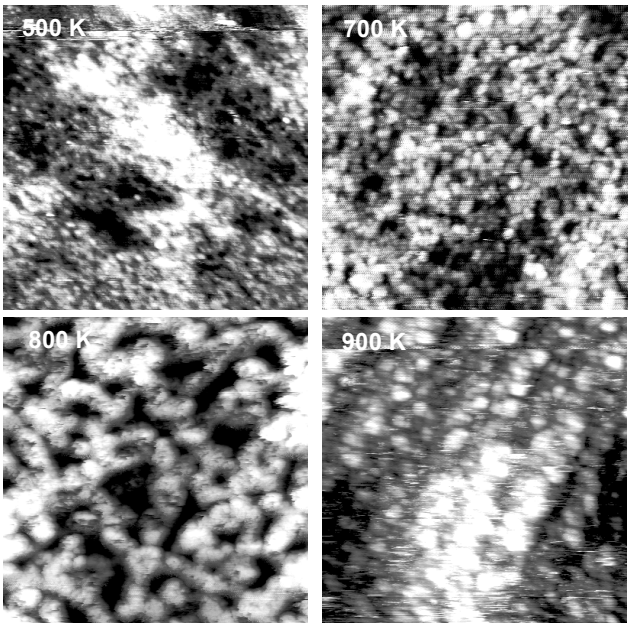

Fig. 4. *STM images of ZnO (0001)-Zn after exposure to 10^{-5} mbar H_2 for 30 min at different temperatures: 500 - 900 K.*

temperature of 800 K to obtain the largest metal surface area of the SiO_2 supported Cu/ZnO system [8], i.e. not relevant for catalysis. The motivation to use this high temperature was to follow the structural changes of ZnO that start at lower temperatures.

The dimensions of the ZnO single crystal, the sample plate and fixing strips were such that the resistance along the surface in the lateral direction and the bulk resistance across the crystal were of similar magnitude, *viz.* 0.3 MΩ. As a consequence, changes of the surface after exposure to H_2 will contribute partially to the STS results. From Fig. 6 it can be seen that the clean initial ZnO surface behaves as an *n*-semiconductor with a flat wide band-gap.

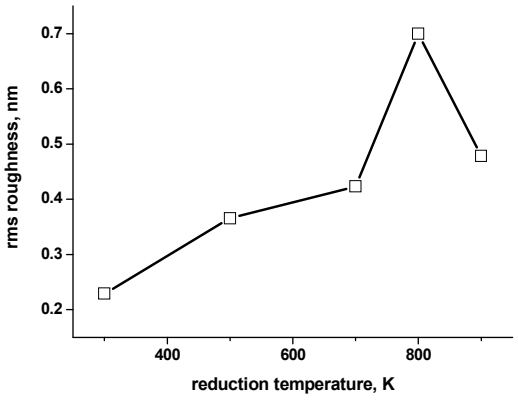

Fig. 5. *Calculated roughness for the surfaces in Fig 4, after the exposure to 10^{-5} mbar H_2 for 30 min at different temperatures.*

Because of the electron conductivity most changes are expected at a negative bias voltage, therefore only this I-V branch is interesting. The I-V curves of the exposed ZnO surface show how the electronic structure changes with the low-pressure reduction temperature from an *n*-semiconducting towards a semi-metallic character (Fig. 6). The inflections for the samples treated at 500 and 700 K may be interpreted as a superposition of the semiconducting subsurface of

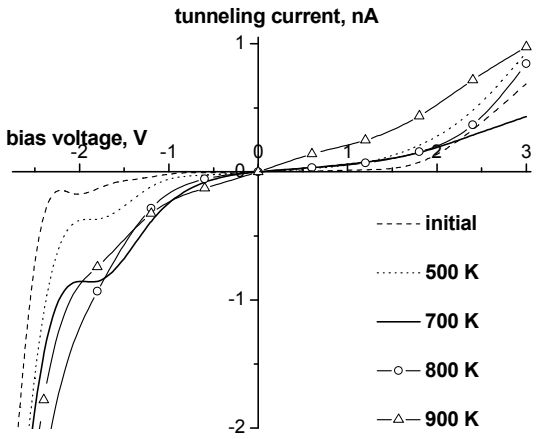

Fig. 6. *I-V curves for the initial clean surface shown in Fig. 3, and the surfaces exposed to 10^{-5} mbar H_2 at 500 - 900 K shown in Fig 4.*

the ZnO crystal and the metallic surface states formed during exposure. The I-V curve obtained after low-pressure reduction at 800 K exhibits a dominating metallic character. The slight shift backwards after treatment at 900 K might be interpreted as the partial removal of the volatile metallic Zn, thereby exposing again the underlying ZnO. The observed metallisation of the oxide surface may have occurred through the reduction of ZnO to metallic Zn and hydroxide, as well as the solution of hydrogen that acts as electron donor.

5.4.2 Reduction at 1 bar H_2

Prior to each treatment samples were subjected to 5 cleaning cycles to restore the Zn-terminated triangular surface structure. Subsequently, the samples were exposed to 1 bar H_2, i.e. a pressure relevant for reaction conditions. A 1 h reduction time was chosen to enable comparison with the silica supported catalysts described by Batyrev *et al.* [8]. In the applied range of reduction temperatures from RT to 800 K, the diffusion coefficient of interstitial hydrogen D_{Hi} in ZnO increases many orders of magnitude from 10^{-21} to 10^{-11} m^2/s [27]. Consequently, hydrogen penetration from the exposed side into the crystal bulk increases to a total loading of more than 30% of the equilibrium value, as calculated from Fourier's second law (Fig. 7).

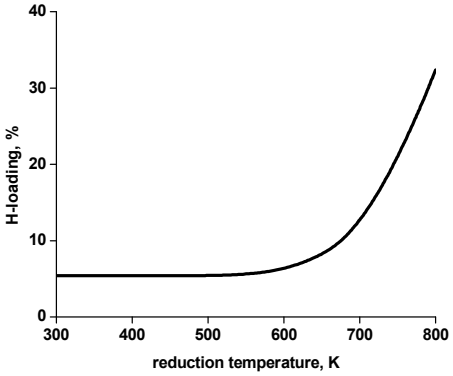

Fig. 7. *Saturation of the ZnO single crystal after 1 h of single-sided exposure to 1 bar H_2 at increasing temperatures, calculated from Fourier's second law and the appropriate diffusion coefficients [27]. Values are expressed as the overall H-loading compared with the equilibrium value at $t = \infty$.*

5.4.3 X-ray Photoelectron Spectroscopy

The intensity ratio of the Zn $2p_{3/2}$ and O 1s peak of the clean Zn-terminated face amounted to 8.4. This value is in good accordance with 8.3 reported by Diebold *et al.* [38].

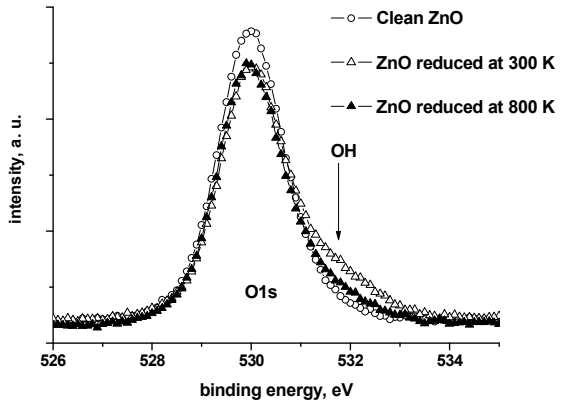

Fig. 8. *Comparison of the XPS spectra of O 1s peak obtained from the clean ZnO surface and those after exposure to 1 bar H_2 at 300 and 800 K.*

After reduction at 1 bar H_2 and RT, formation of OH groups at the ZnO surface is observed in XPS as a pronounced shoulder at the high energy side of the O 1s peak at ~ 531.7 eV (Fig. 8). At the same time the O 1s peak height has decreased some 12% compared to untreated ZnO. This can be attributed partly to the increased surface roughness, since the Zn $2p_{3/2}$ peak height had decreased 9% (result not shown). As a consequence, the Zn/O peak ratio after reduction amounted to 8.7, which is indicative of the balancing surface metallisation according to reaction (1).

After reduction at 1 bar H_2 and 800 K the hydroxide shoulder has gone, which might be understood from the fact that *bulk* $Zn(OH)_2$ starts to decompose at 375 K. The height of the O 1s peak remained unchanged, while the height of the Zn $2p_{3/2}$ peak increased. The resulting Zn/O peak ratio of 9.0 is clearly indicative of substantial metallisation of the ZnO surface after high temperature reduction and in good accordance with the STS results.

5.4.4 Thermal desorption spectroscopy

Thermal desorption spectroscopy (TDS) is a useful technique in model studies to analyse the desorbed products from single crystals [39, 40]. In this case TDS was used to study metallisation of the ZnO

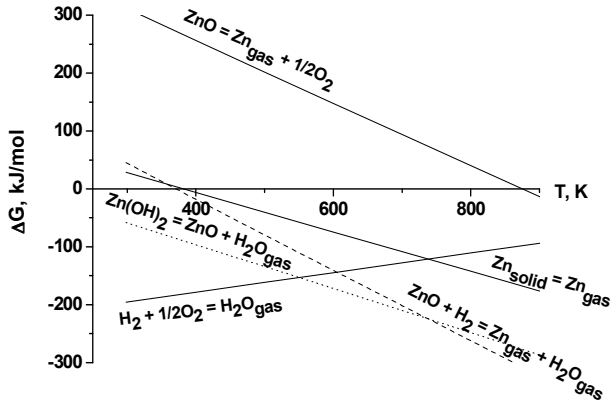

Fig. 9. *Gibbs free energies of relevant reactions at a typical pressure of 10^{-9} mbar during annealing, calculated from available data on ΔG_0 and $c_p(T)$ [37, 43]. Dashed line: unsteady-state reduction of ZnO by dissolved H_2 at 1 bar and gaseous products at 10^{-9} mbar as encountered during annealing in UHV after the preceding reduction step.*

surface after reduction. To enable interpretation of the results, Gibbs free energies of the relevant reactions at a typical pressure of 10^{-9} mbar were calculated from available thermodynamic data and are presented in Fig. 9.

When the untreated ZnO(0001)-Zn crystal was heated a relatively strong H_2 signal with a maximum of 10 nA was obtained. Most likely this hydrogen was introduced during the growth of the crystal by the hydrothermal method, as reported elsewhere [41, 42].

After 1 h exposure to 1 bar H_2 at 300-800 K, thermal desorption spectra of H_2, H_2O, O_2 and Zn were obtained simultaneously. During annealing the total pressure typically increased from $3.0 \cdot 10^{-10}$ mbar at RT to $4.5 \cdot 10^{-9}$ mbar at 550 K, while at 1000 K it has reduced again to about $1.5 \cdot 10^{-9}$ mbar. This course of the pressure with time and temperature is determined by the balance between desorption and pumping rate.

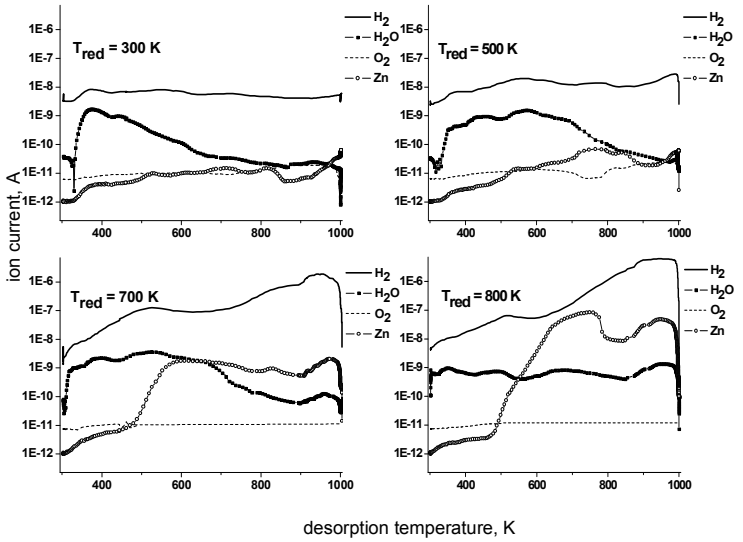

Fig. 10. *Thermal desorption spectra of the ZnO surface after exposure to 1 bar H_2 at different temperatures. The vertical lines at the end represent the hold-period after the final temperature was reached. Please note the logarithmic vertical scale.*

H_2, O_2, H_2O and Zn are the main desorption products from the reduced ZnO surface; their thermal desorption spectra are plotted in Fig. 10. The high and rather constant hydrogen level after reduction at RT is indicative of the low pumping rate of this light molecule by the turbo-molecular pump [40]. The differences in hydrogen

desorption spectra between RT and the higher reduction temperatures, however, must be ascribed to interstitial hydrogen H_i released from the ZnO matrix. The increase of the hydrogen signal by 3 orders of magnitude with the applied reduction temperature implies modification of the ZnO crystal to a larger extent, and may be understood from the abovementioned increase of the interstitial diffusion coefficient (Fig. 7).

The water signal displays a fast increase upon annealing for all reduction temperatures and has a maximum around 375 K. From the subsequent exponential decrease after reduction at RT it is obvious that this water peak originates from a limited source. Therefore, it is assigned to the decomposition of the hydroxyl groups at the outermost ZnO surface:

$$Zn(OH)_2 \Rightarrow ZnO + H_2O\ (g) \qquad (2)$$

It should be noted that at 10^{-9} mbar bulk $Zn(OH)_2$ already starts to decompose at 150 K (Fig. 9). The net effect of the surface hydroxyl formation during the reduction (1) and the removal of water during annealing (2) will be that some 25% of the ZnO surface is reduced to metallic Zn. This finding implies that hydroxyl groups play no role in the synthesis of methanol at a typical reaction temperature of 500 K.

The H_2O signal that saturates around 10^{-9} A during desorption from ZnO reduced at higher temperatures must be due to water formation at a rate that compensates the pumping speed. Therefore, the increasing amounts of water found at annealing temperatures > 500 K after reduction at 500-800 K are thought to be produced *in situ* from ZnO at the surface and desorbing H_i, leading to the *overall* reaction:

$$ZnO + H_2 \Rightarrow Zn\ (g) + H_2O\ (g) \qquad (3)$$

Under UHV conditions reduction of ZnO may indeed occur at these temperatures for two reasons: (i) during the unsteady desorption state in UHV, the thermodynamic potential of the dissolved interstitial H_i is still close to the thermodynamic potential of H at 1 bar of H_2 gas, and (ii) the Zn pressure will be very low due to sublimation on the cold walls. As a consequence, annealing of the H-loaded ZnO crystal in UHV is comparable to reduction in a H_2 stream that dilutes the products. This implies that the conditions of our TDS measurements are the equivalent of monitoring the 1 bar reduction process by means of a leak-in mass spectrometer. Using standard conditions for the reactants and 10^{-9} mbar for the products in the thermodynamic calculations indicates that *in situ* reduction (3) may occur from 400 K onwards (Fig. 9).

The oxygen signal during desorption from the sample treated at RT remains at a constantly low 10^{-11} A, an order of magnitude

typical of the background in the UHV system. Oxygen in excess of this level will immediately form water under the prevailing reducing conditions, *viz.* 10^{-9} mbar and T < 1450 K (Fig. 9). Therefore, the strongly coupled mass 32 and 64 signals obtained after reduction at 700-800 K and annealing temperatures > 500 K were not attributed to $^{32}O_2^{1+}$ and $^{64}Zn^{1+}$, but to $^{64}Zn^{2+}$ and $^{64}Zn^{1+}$.

After reduction at RT the zinc signal starts as low as $4 \cdot 10^{-13}$ A, and gradually increases about 1 order of magnitude upon annealing due to sublimation of a small amount of metallic Zn from the surface. Note that at 10^{-9} mbar Zn starts to sublimate at 375 K (Fig. 9). After reduction at 700 K a major and stepwise increase of the Zn signal is observed when annealing at 420-520 K. This reflects the large increase of the H-loading that occurs at reduction temperatures > 600 K (Fig. 7), and the subsequent enhancement of the *in situ* reduction by H_i. A larger and more extended effect is observed during annealing of the crystal reduced at 800 K.

Furthermore, after reduction at these high temperatures a distinct Zn peak can be observed at 880-980 K. This might be explained by the direct decomposition:

$$ZnO \Rightarrow Zn\ (g) + \tfrac{1}{2}O_2\ (g) \qquad (4)$$

which at 10^{-9} mbar occurs at 875 K (Fig. 9). At the prevailing H_2 levels, the associated oxygen is immediately reduced (see the corresponding H_2O peak). So in this case ZnO is reduced according to a sequential reaction that differs from the *in situ* mechanism that occurs at the higher H_i levels present during the earlier stage of the annealing process.

When the annealed samples were kept at 1000 K for 30 minutes, H_2, O_2 and H_2O signals decreased to the initial values at RT. Although the Zn signal also decreases a few orders of magnitude, the final level remains about ten times higher than at RT. This suggests that direct decomposition (4) still proceeds, but at a much lower rate after all absorbed forms of H (3) have gone. An explanation might be that the crystalline ZnO (0001) is exposed again after removal of the layers affected by H_i [29]. The depth of the involved layers can be estimated from e.g. the integrated amount of desorbed Zn. Assuming half of the sublimated Zn reaches the mass-spectrometer, some 20-80 monolayers were removed during annealing of the samples reduced at 700-800 K.

From a catalytic point of view we conclude that under typical reduction conditions of 700-750 K metallic Zn will be formed at the ZnO (0001) surface. The degree of metallisation will be rather limited, since the volatile Zn may start to sublimate even at lower temperatures, depending on the partial pressure in the gas phase. This

implies that prolonged reduction or reduction at higher temperatures will only lead to loss of material.

The increase of the calculated H-loading after reduction at RT and 800 K amounts to a factor of 6 (Fig. 7), but the observed H desorption increases a 1000 times (Fig. 10). From this comparison it is obvious that metallic Zn greatly enhances dissociative adsorption of H_2, and underlines the importance of ZnO as an atomic H supplier by spillover.

Reduction of ZnO and sublimation of Zn in a SiO_2-supported system was found to occur at 750 and 800 K, respectively [8]. These temperatures are 250-300 K higher than those used in the present TDS results on the ZnO single crystal and illustrate the high stability of a nano-crystalline ZnO phase under reducing conditions.

5.5 Conclusions

The clean ZnO (0001)-Zn terminated crystal face was studied by STM and STS. In UHV the surface consists of triangular pits and islands of various sizes with a monolayer step height. After exposure to 10^{-5} mbar H_2 at RT this reconstruction is lifted and a rough surface forms. The roughness as well as the metallic character of the surface increased with the applied low-pressure reduction temperature up to 800 K. The observed roughening of the single crystal ZnO is considered relevant also for ZnO supported catalysts, as it will increase the surface area and therefore the number of exposed low-index planes.

XPS revealed that exposure to 1 bar H_2 at RT led to the formation of OH groups; at higher temperatures progressive metallisation of the ZnO surface was found.

Analysis of the TDS results showed that huge amounts of H_2 dissolved into the ZnO crystal. Its unsteady-state desorption during annealing in UHV enabled to monitor the reduction process *in situ* at low partial pressures of the products. The results obtained under these conditions agree well with thermodynamic calculations. Formation of hydroxide at RT was evidenced from its decomposition at 375 K. Reduction of ZnO and subsequent sublimation of metallic Zn started around 500 K. As a consequence, the degree of surface metallisation in ZnO supported catalysts is expected to lie within narrow limits. Direct decomposition of ZnO started at 880 K at a rate that decreased strongly with time. The latter finding is attributed to the ultimate removal of ZnO layers affected by dissolved interstitial H.

The experimental ratio between the absorbed amount of H_2 at RT and 800 K amounts to 1000. The ratio calculated from increasing diffusion coefficients with temperature only amounts to 6. This

emphasizes the importance of ZnO as an atomic H supplier by spillover, and proves that metallic Zn boosts dissociative adsorption of H_2.

Finally, we emphasise that metallisation of the ZnO surface was established by all the experimental techniques employed. It is expected that the associated O vacancies mediate the adsorption step of CO/CO_2 from syngas.

References

1. R.G. Hermann, K. Klier, G.W. Simmons, B.P. Finn, and J.B. Bulko, *J. Catal.*, 1979, 56, 407.
2. R. Burch, S.E. Golunski, and M.S. Spencer, *J. Chem. Soc., Faraday Trans.*, 1990, 86, 2683.
3. M.S. Spencer, *Catal. Lett.*, 1998, 50, 37.
4. J. Yoshihara and C.T. Campbell, *J. Catal.*, 1996, 161, 776.
5. B.S. Clausen, J. Schiøtz, L. Gråbæk, C.V. Ovesen, K.W. Jacobsen, J.K. Nørskov, and H. Topsøe, *Topics in catalysis*, 1994, 1, 367.
6. S.A. French, A.A. Sokol, S.T. Bromley, C.R.A. Catlow, S.C. Rogers, F. King, and P. Sherwood, *Angew. Chem. Int. Ed.*, 2001, 40, 4437.
7. T. Fujitani and J. Nakamura, *Appl. Catal. A* , 2000, 191, 111.
8. E.D. Batyrev, J.C. van den Heuvel, J. Beckers, W.P.A. Jansen, and H.L. Castricum, *J. Catal.*, 2005, 229, 136.
9. M. Bowker, H. Houghton, and K.C. Waugh, *J. Chem. Soc., Faraday Trans.*,1982, 178, 2573.
10. J.M. Vohs and M.A. Barteau, *J. Phys. Chem.*, 1987, 91, 4766.
11. V.E. Henrich and P.A. Cox, *Cambridge University Press: The surface science of metal oxides*, 1994, Cambridge.
12. G. Kresse, O. Dulub, and U. Diebold, *Phys. Rev. B*, 2003, 68, 245409.
13. M. Valtiner, S. Borodin, and G. Grundmeier, *Phys. Chem. Chem. Phys.*, 2007, 9, 2406.
14. Th. Becker, St. Hövel, M. Kunat, Ch. Boas, U. Burghaus, and Ch. Wöll, *Surf. Sci.*, 2001, 486, L502.
15. N. Fujimura, T. Nishihara, S. Goto, J. Xu, and T. Ito, *J. Crystal Growth*, 1993, 130, 269.
16. O. Dulub, L.A. Boatner, and U. Diebold, *Surf. Sci.*, 2002, 519, 201.
17. F. Ostendorf, S. Torbrügge, and M. Reichling, *Phys. Rev. B*, 2008,77, 041405.
18. P.W. Tasker, *J. Phys. C: Solid State Phys.*, 1979, 12, 4977.
19. G.C. Benson and K.S. Yun, *Arnold: The solid gas interface, Ed. E.A. Flood*, 1967, London.

20. R.W. Nosker, P. Mark, and J.D. Levine, *Surf. Sci.*, 1970, 19, 291.
21. O. Dulub, U. Diebold, and G. Kresse, *Phys. Rev. Lett.*, 2003, 90, 016102-1.
22. N. Jedrecy, M. Sauvage-Simkin, and R. Pinchaux, *Appl. Surf. Sci.*, 2000, 162-163, 69.
23. S. Torbrügge, F. Ostendorf, and M. Reichling, *J. Phys. Chem. C*, 2009, 113, 4909.
24. D.G. Thomas and Y.Y.Lander, *J. Chem. Phys.*, 1956, 25, 1136.
25. R. Lindner, *Acta Chem Scand.*, 1952, 6, 457.
26. W.J. Moore and E.L.Williams, *Discuss. Faraday Soc.*, 1959, 28, 86.
27. I. Kuzmina and V.A. Nikitenko, *Nauka: Zinc oxide, synthesis and optical properties*, 1984, Moscow.
28. D.C. Look, *Phys. Rev. Lett.*, 1999, 82, 2552.
29. C.G. van de Walle, *Phys. Rev. Lett.*, 2000, 85, 1012.
30. V.L. Bonch-Bruevich and S.G. Kalashnikov, *Nauka: Physics of Semiconductors*, 1977, Moscow.
31. C.T. Au, W. Hirsch, and W. Hirschwald, *Surf. Sci.*, 1988, 199, 507.
32. M.F. Guimon, G. Pfister-Guillouzo, M. Bremont, W. Brockmann, C. Quet, and J.Y. Chenard, *Appl. Surf. Sci.*, 1997, 108, 149.
33. A. Wander, F. Schedin, P. Steadman, A. Norris, R. McGrath, T.S. Turner, G. Thornton, and N.M. Harrison, *Phys. Rev. Lett.*, 2001, 86, 3811.
34. T.M. Parker, N.G. Condon, R. Lindsay, F.M. Leibsle, and G. Thornton, *Surf. Sci.*, 1998, 415, L1046.
35. B. Hoffmann-Millack, *Omicron Nano Technology GmbH: Multiprobe XP Omicron system manuals*, 1997, Taunusstein.
36. A.N. Mariano and R.E. Hanneman, *J. Appl. Phys.,* 1963, 34, 384.
37. D.R. Lide and H.P.R. Frederikse, *CRC Press: CRC handbook of chemistry and physics, 76th ed.*, 1995, Boca Raton FL.
38. U. Diebold, L.V. Koplitz, and O. Dulub, *Appl. Surf. Sci.*, 2004, 237, 336.
39. J.L. Falconer and J.A.Schwarz, *Catal. Rev. Sci. Eng.*, 1983, 25, 141.
40. J.W. Niemantsverdriet, *Willey-VCH: Spectroscopy in Catalysis, 2nd ed.*, 2000, Weinheim.
41. E.D. Kolb and R.A. Laudise, *J. Amer. Ceram. Soc.*, 1966, 49, 302.
42. R.A. Laudise and A. Ballman, *J. Phys. Chem.*, 1960, 64, 688.
43. A. Paul and H.N. Acharya, *J. Material Sci.*, 1992, 27, 1716.